Supporting Information for

"Insights on the electron-donating and withdrawing effect of the functional groups on mechanochemical dehydrochlorination reactions"

Fang Guo,*[a] Zhen Wang,[a] Jin-Jing Zhang[a] Antonino Famulari,[b] Hai-tao Li[a] and Javier Martí-Rujas[c]*

a College of Chemistry, Liaoning University, Shenyang 110036, China.

b Dipartimento di Chimica Materiali e Ingegneria Chimica. ''Giulio Natta'', Politecnico di Milano, Via L. Mancinelli 7, 20131 Milan, Italy.

c Center for Nano Science and Technology@Polimi, Istituto Italiano di Tecnologia, Via Pascoli 70/3, 20133 Milano, Italy.

Content

Preparation of L_2

Figure S6. ^{13}C NMR plot corresponding to **L2.**

Figure S7. Mass spectrometry analysis plot of **L2**.

Single crystal X-ray structure of L_2

Figure S8. Single crystal X-ray structure showing one molecule of **L2**.

Figure S9. Single crystal X-ray structure showing the packing of **L2** viewed along the *b*-axis.

Figure S10. Simulated XRPD pattern of **L2** obtained from its single crystal X-ray structure.

Figure S11. Crystal structure of **1'** showing the pockets (yellow), corresponding to the volume occupied by the included guest molecules after LAG reaction in the transformation from a second coordination sphere adduct (**1**) into a coordination complex (**1'**).

Figure S12. Experimental XRPD of second sphere adduct **1** obtained upon grinding (a) and simulated from its single crystal X-ray structure determination (b).

Figure S13. Crystal structure of **3** showing the *quasi*-chelating interaction between the cation and anion. Hydrogen bonding interactions are shown in black dashed lines.

Figure S14. Crystal structure of **3** viewed along the *b*-crystallographic axis.

Figure S15. Simulated XRPD pattern of **3** obtained from its single crystal X-ray structure.

Dehydrochlorination reactions by liquid assisted grinding (LAG).

Figure S16. Crystal structure of **4** showing the *quasi*-chelating interaction between the cation and anion. Hydrogen bonding interactions are shown in black dashed lines.

Figure S17. Crystal structure of **4** viewed along the *b*-crystallographic axis.

Figure S18. Simulated XRPD pattern of **4** obtained from its single crystal X-ray structure.

Figure S19. Crystal structure of **5** showing the *quasi*-chelating interaction between the cation and anion. Hydrogen bonding interactions are shown in black dashed lines.

Figure S20. Crystal structure of **5** viewed along the *b*-crystallographic axis.

Figure S21. Simulated XRPD pattern of **5** obtained from its single crystal X-ray structure.

Figure S22. a) Experimental XRPD pattern of **L2**. (b). LAG of **2** with KOH for 5s. (c). LAG of **2** with KOH for 10s. The product is amorphous.

Figure S23. Experimental XRPD pattern of **L2**. (b) LAG of **2** with K_2CO_3 for 5s. (c) LAG of **2** with K_2CO_3 for 10s. (d) LAG of **2** with K_2CO_3 for 15s. (e) LAG of **2** with K_2CO_3 for 20s.

Figure S24. (a) Experimental XRPD pattern of **L2**. (b) Experimental pattern of block new polymorph of ligand **L2** (beta phase). (c) LAG of **3** with KOH for 5s. (d) LAG of **3** with KOH for 10s. (e) LAG of **3** using KOH for 15s.

Figure S25. (a) Experimental pattern of **L2**. (b) Experimental pattern of new polymorph. (c) LAG of **3** with K_2CO_3 for 5s. (d) LAG of **3** grind with K_2CO_3 for 10s. (e) LAG of **3** grind with K_2CO_3 for 15s.

Figure S26. (a) Experimental XRPD pattern of ligand **L2**. (b) LAG of **4** with KOH for 5s. (c) LAG of **4** with KOH for 10s.

Figure S27. (a) Experimental XRPD pattern of ligand **L2**. (b) LAG of **4** with K_2CO_3 for 5s. (c) LAG of **4** with K_2CO_3 for 10s. (d) LAG of **4** with K_2CO_3 for 15s.

Figure S28. (a) Experimental XRPD pattern of ligand **L2**. (b) LAG of **5** with KOH for 5s. (c). LAG of **5** with KOH for 10s. (d) LAG of **5** using KOH for 15s.

Figure S29. (a) Experimental XRPD pattern of ligand **L2**. (b) LAG of **5** with K_2CO_3 for 5s. (c) LAG of **5** using K_2CO_3 for 10s. (d) LAG of **5** with K_2CO_3 for 15s.

Materials and Methods

All chemicals were obtained from commercial sources and used without further purification. IR spectra were obtained with a PerkinElmer 100 FT-IR spectrometer using KBr pellets. ^{1}H NMR and ^{13}C NMR spectra were recorded on a Mercury-Plus 300 spectrometer (Varian, 300 MHz) at 25 °C with tetramethylsilane as the internal reference. High resolution mass spectrometry (HRMS) experiments were carried out on an Agilent 1100 Series SL ion trap mass spectrometer (Agilent Technologies, Santa Clara, CA, USA) with an eletrospray ionization interface in positive and negative ion detection mode. The voltage of the capillary tube at the entrance was 3500 V, the nebulizer nitrogen gas pressure was set at 30psi and the drying nitrogen gas rate was set at 8.0 L/min. Drying gas temperature was 325℃. The voltage of collision-induced dissociation with helium buffer gas was 1.0 V. The scan range was 0-1000 m/z.

X-ray Crystallography

Single crystal X-ray diffraction (SC-XRD) experiments of crystals **1**, **1'**, **3**, **4** and **5** were carried out using a Bruker P4 diffractometer (Mo-Kα radiation, λ = 71073 Å.) The single crystal X-ray data collection of crystal **2** was recorded using a Bruker X8 Prospector APEX-II/CCD diffractometer equipped with a focusing mirror (Cu-Kα radiation, λ = 1.54056 Å) at the Center for Nano Science and Technology@PoliMi.

The structures were determined using direct methods and refined (based on F2 using all independent data) by full-matrix least-square methods (SHELXTL 97).[1] All non-hydrogen atoms were located from different Fourier maps and refined with anisotropic displacement parameters. All the structures were refined by full-matrix least-squares methods using ShelXL-2014/7.[2]

X-ray powder diffraction (XRPD) data were carried out using a Bruker D8 ADVANCE X-ray powder diffractometer (Cu-Kα radiation, λ = 1.54056 Å). All the experiments were carried out at room temperature.

Preparation of L_1

Ethylenediamine (7 mL) was slowly added into a solution of 8 g NaOH and 20 mL distilled water. *p*-methylbenzyl chloride (30 mL; 2-3 drops/sec) was then continuously added into the mixture solution. After the reaction was heated to 95 °C and stirred for 4 h, the mixture was cooled to room temperature. The white reaction product was washed with distilled water. Recrystallization using anhydrous ethanol and drying in vacuo, produced white crystals 18.5 g, yield 77%. M. p. 95-97°C.

^{1}H NMR ($CDCl_3$, 300MHz) δ: 7.05-7.16 (8H, m, ArH), 3.45 (4H, s, CH_2), 2.57 (2H, s, CH_2), 2.32 (6H, s, CH_3).

^{13}C NMR (75 MHz, $CDCl_3$): δ 136.6 (s, C_a), 136.1 (s, C_b), 128.7 (s, C_c), 128.7 (s, C_d), 58.1 (s, C_e), 50.9 (s, C_f), 21.1 (s, C_g).

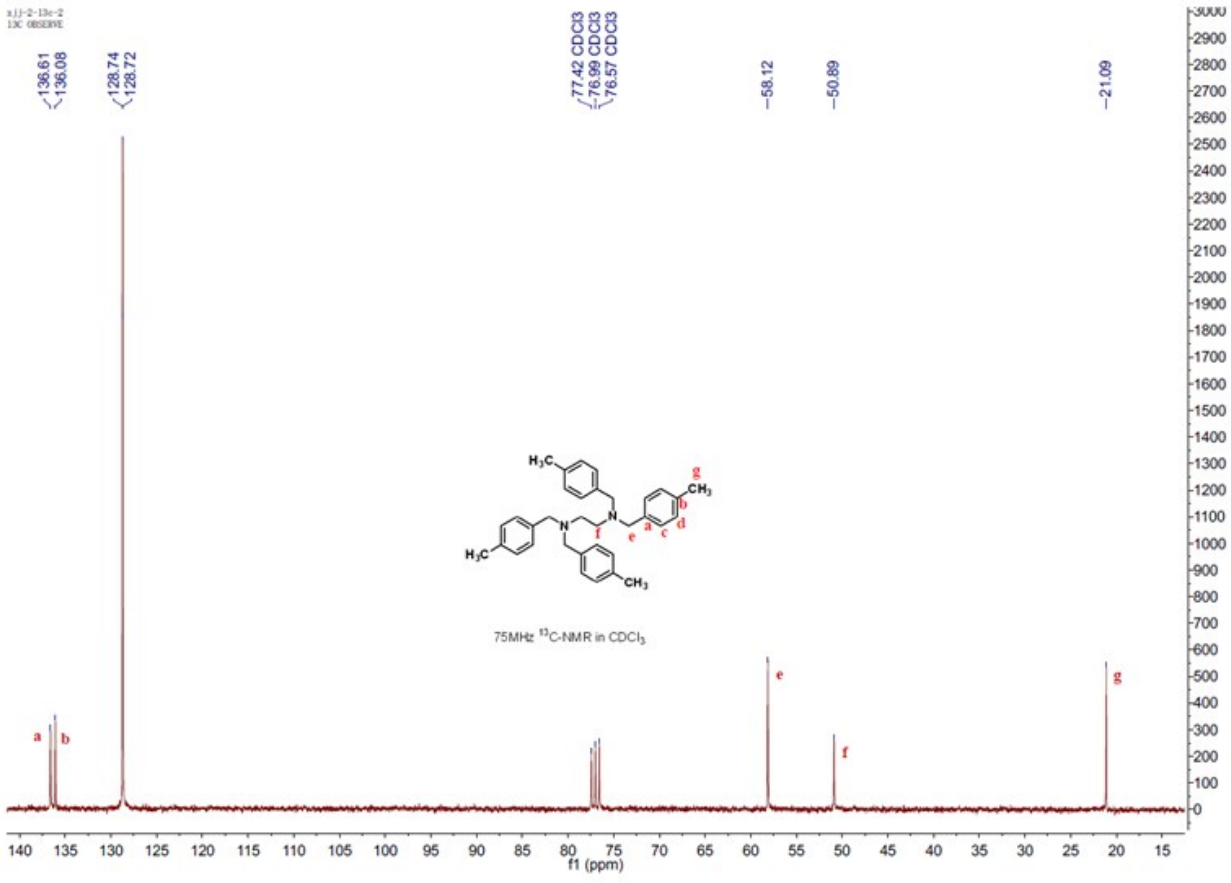

Figure S1. ^{13}C NMR plot corresponding to **L1.**

Mass Spectrometry Analysis: calcd (m/z) for $C_{34}H_{41}N_2$: 477.3 ($[M + H]^+$), found: 477.4 ($[M + H]^+$).

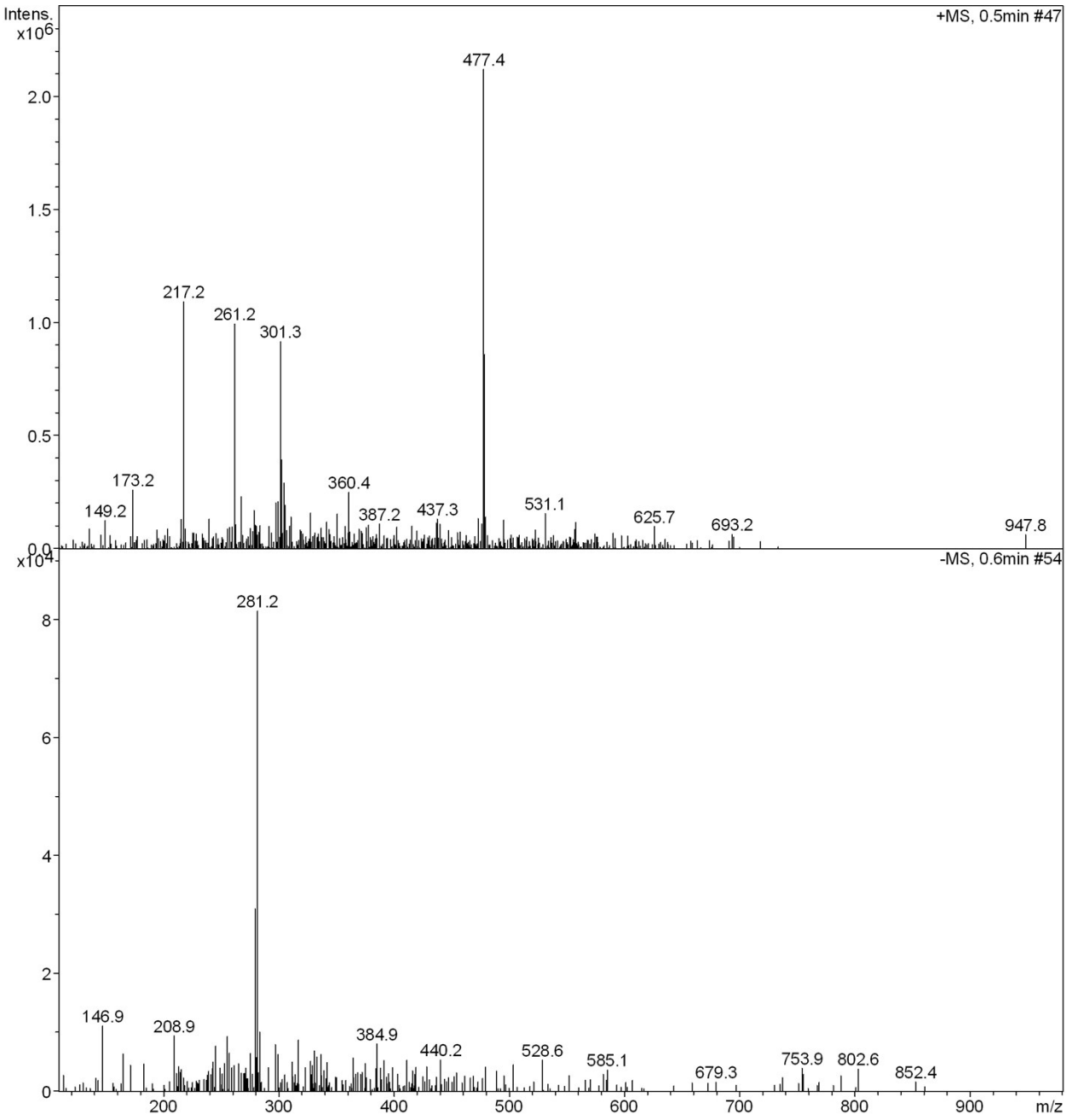

Figure S2. Mass spectrometry analysis plot of **L1**.

Single crystal X-ray structure of L_1

Single crystals of **L1** were obtained by evaporating from appropriate solvent. In **L1** there are two half molecules of **L1** in the asymmetric unit corresponding to two different conformations of the ligand in the crystalline state. It crystallizes in the $P2_1/c$ monoclinic space group.

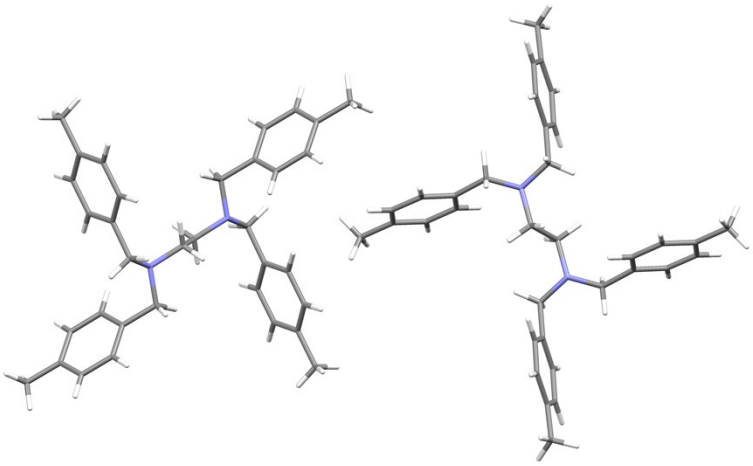

Figure S3. Single crystal X-ray structure showing two molecules of **L1**.

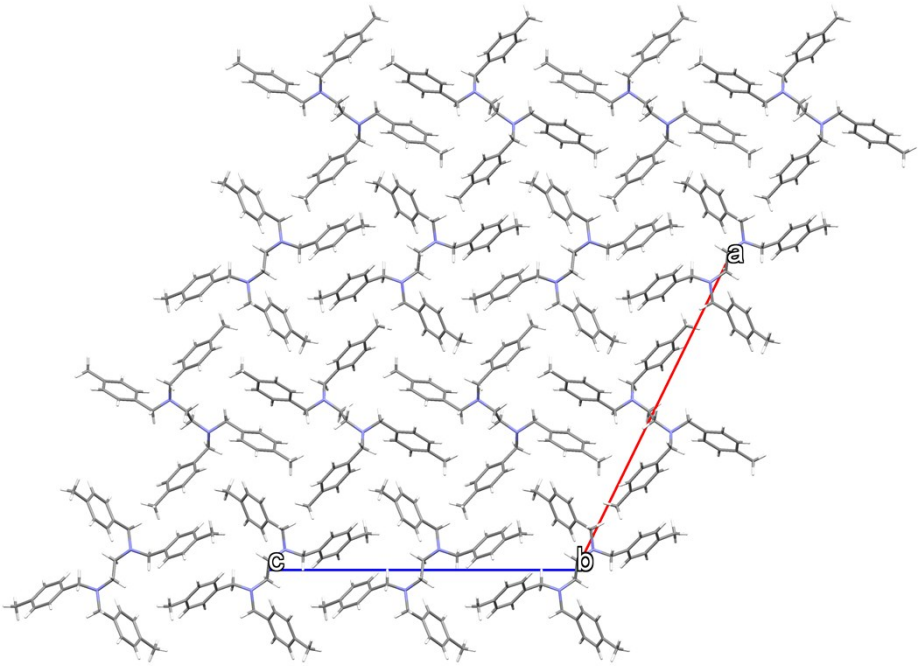

Figure S4. Single crystal X-ray structure showing the packing of **L1** viewed along the *b*-axis.

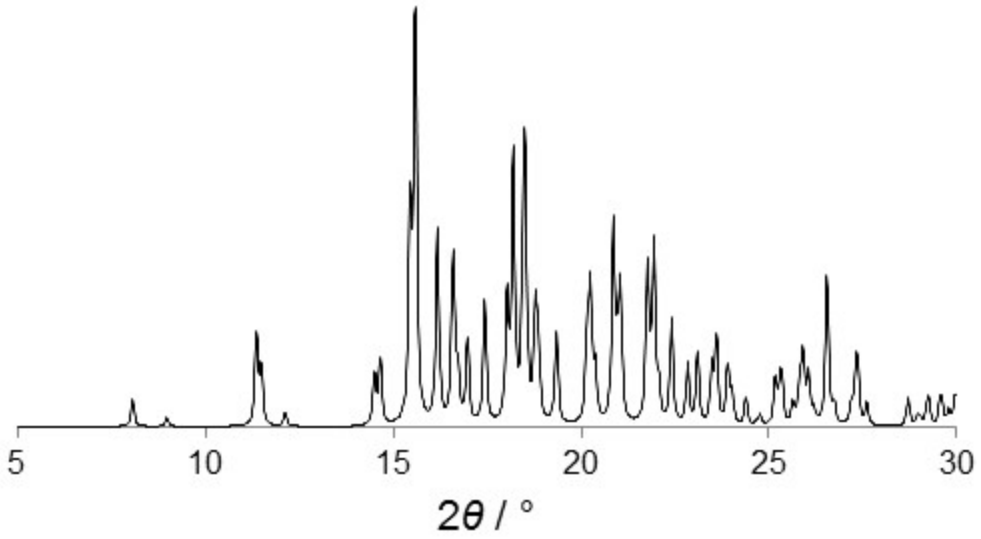

Figure S5. Simulated XRPD pattern of **L1** obtained from its single crystal X-ray structure.

Preparation of L_2

Ethylenediamine 2.0 ml (0.033mol) was slowly added into a solution of 6.0 g NaOH (0.15ol) in 20 ml distilled water. Then 20ml (0.135 mol) 4-trifluoromethylbenzyl was continuously added into the mixture solution. The reaction was then heated to 45 °C and stirred for 4 h. After the mixture was cooled to room temperature, the white product was separated with distilled water. Recrystallization using anhydrous ethanol and drying in vacuo, produced white crystals 1.0523 g, 64.12%. M.p. 83-85°C.

^{1}H-NMR ($CDCl_3$, 300 MHz) δ: 7.30–7.61 (16H, m, ArH), 3.57 (8H, s, CH_2), 2.53 (4H, t, CH_2).

^{13}C NMR (75 MHz, $CDCl_3$): δ 143.4 (4×C, s, C_a), 129.4 (4×C, q, J = 32.3 Hz, C_b), 128.7 (8×C, s, C_c), 125.2 (8×C, q, J = 3.8 Hz, C_d), 124.1 (4×C, q, J = 270 Hz, C_e), 58.5 (4×C, s, C_f), 51.7 (2×C, s, C_g).

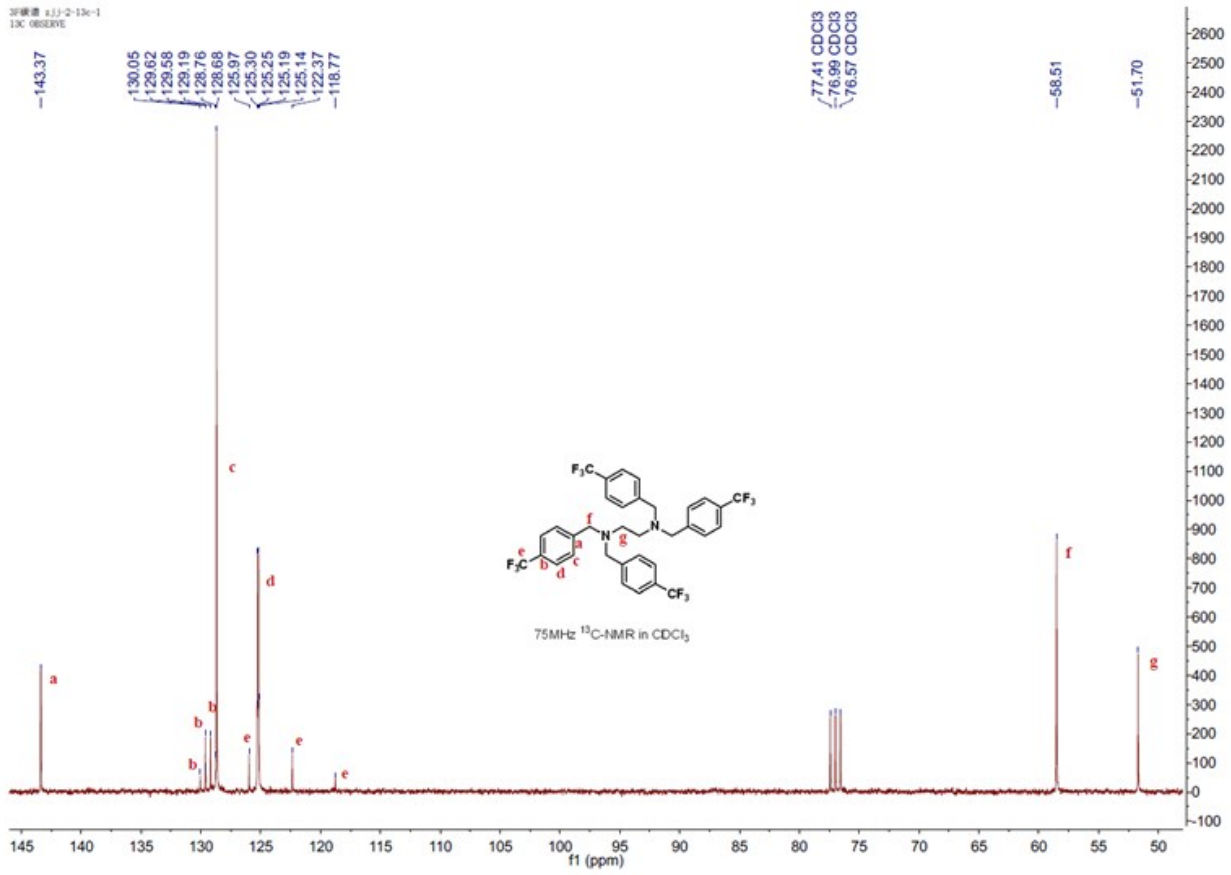

Figure S6. ^{13}C NMR plot corresponding to **L2.**

Mass Spectrometry Analysis: calcd (m/z) for $C_{34}H_{29}F_{12}N_2$: 693.2 ($[M + H]^+$), found: 693.3 ($[M + H]^+$).

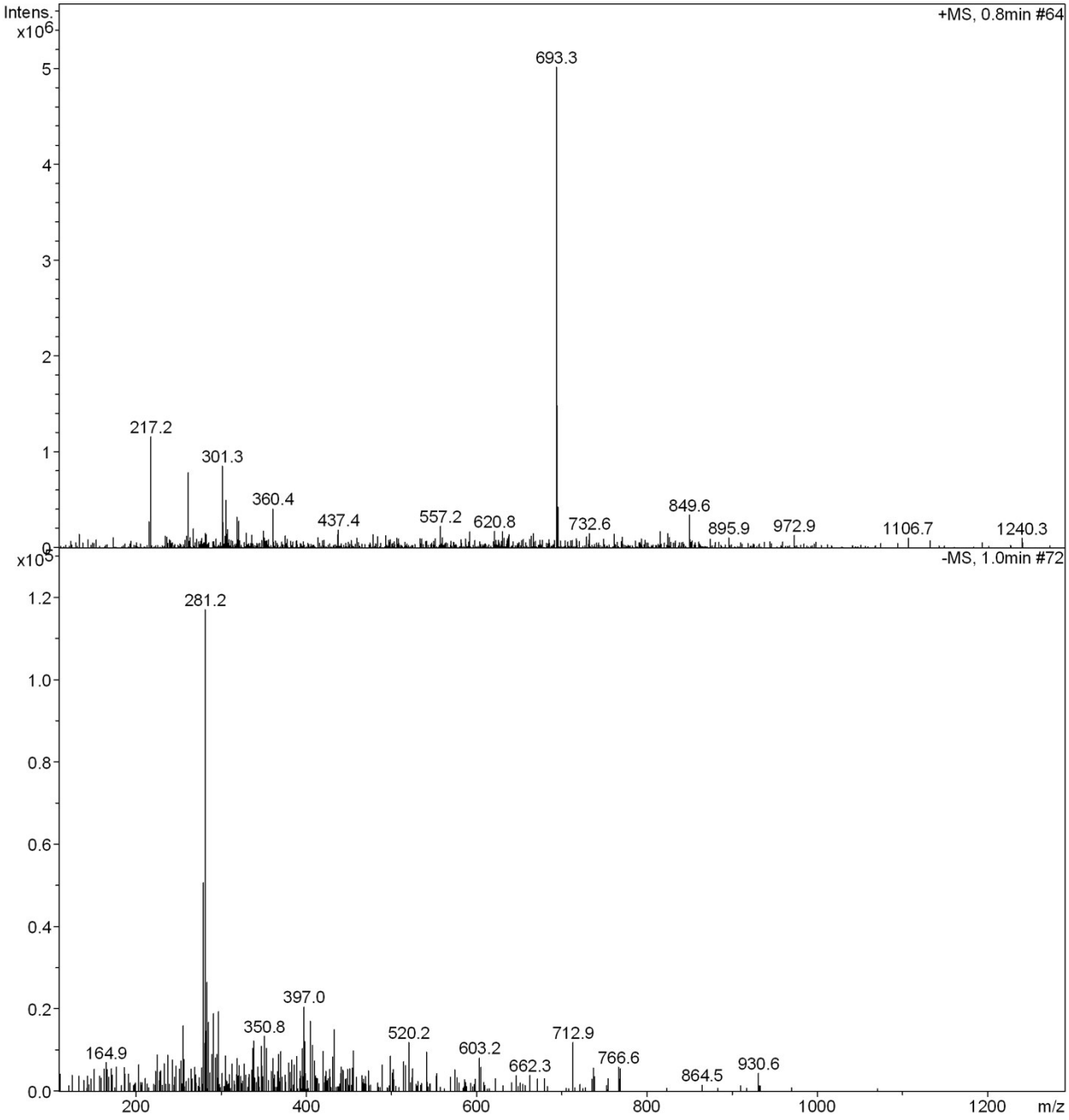

Figure S7. Mass spectrometry analysis plot of **L2**.

Single crystal X-ray structure of L_2

The crystal structure of **L2** consists of half molecule of L2 in the asymmetric unit and it does not contain solvent. The molecule of **L2** is in an extended conformation. It crystallizes in the $P2_1/n$ monoclinic space group.

Note: We have detected a new polymorph of **L2** depending on the crystallization conditions. This will be reported in an upcoming article.

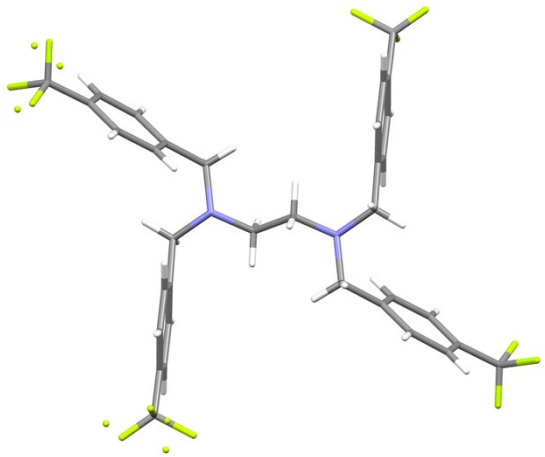

Figure S8. Single crystal X-ray structure showing one molecule of **L2**.

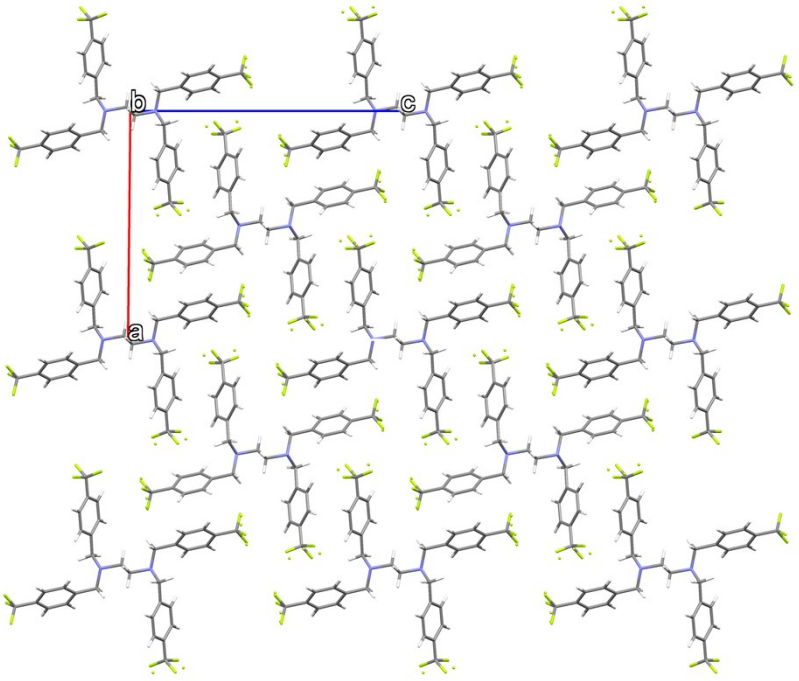

Figure S9. Single crystal X-ray structure showing the packing of **L2** viewed along the *b*-axis.

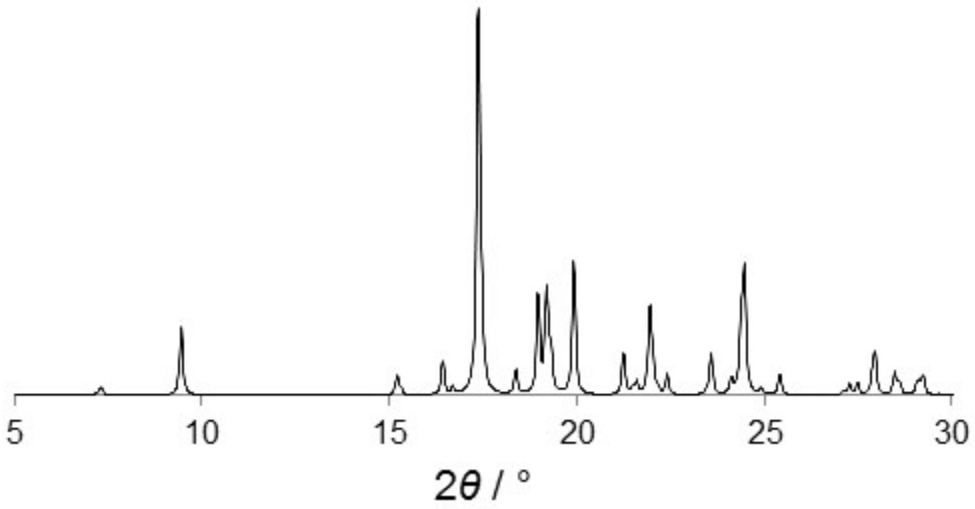

Figure S10. Simulated XRPD pattern of **L2** obtained from its single crystal X-ray structure.

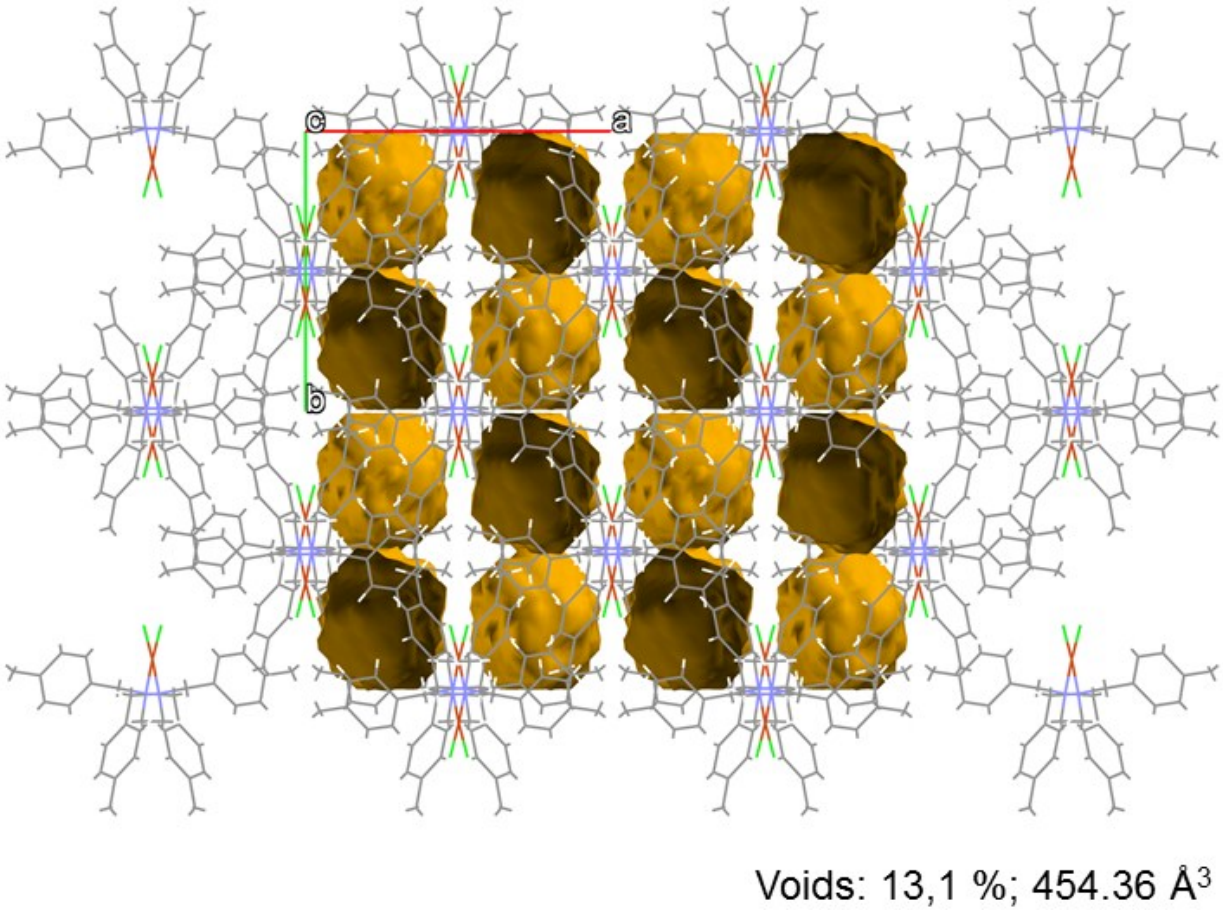

Figure S11. Crystal structure of **1'** showing the pockets (yellow), corresponding to the volume occupied by the included guest molecules after LAG reaction in the transformation from a second coordination sphere adduct (**1**) into a coordination complex (**1'**).

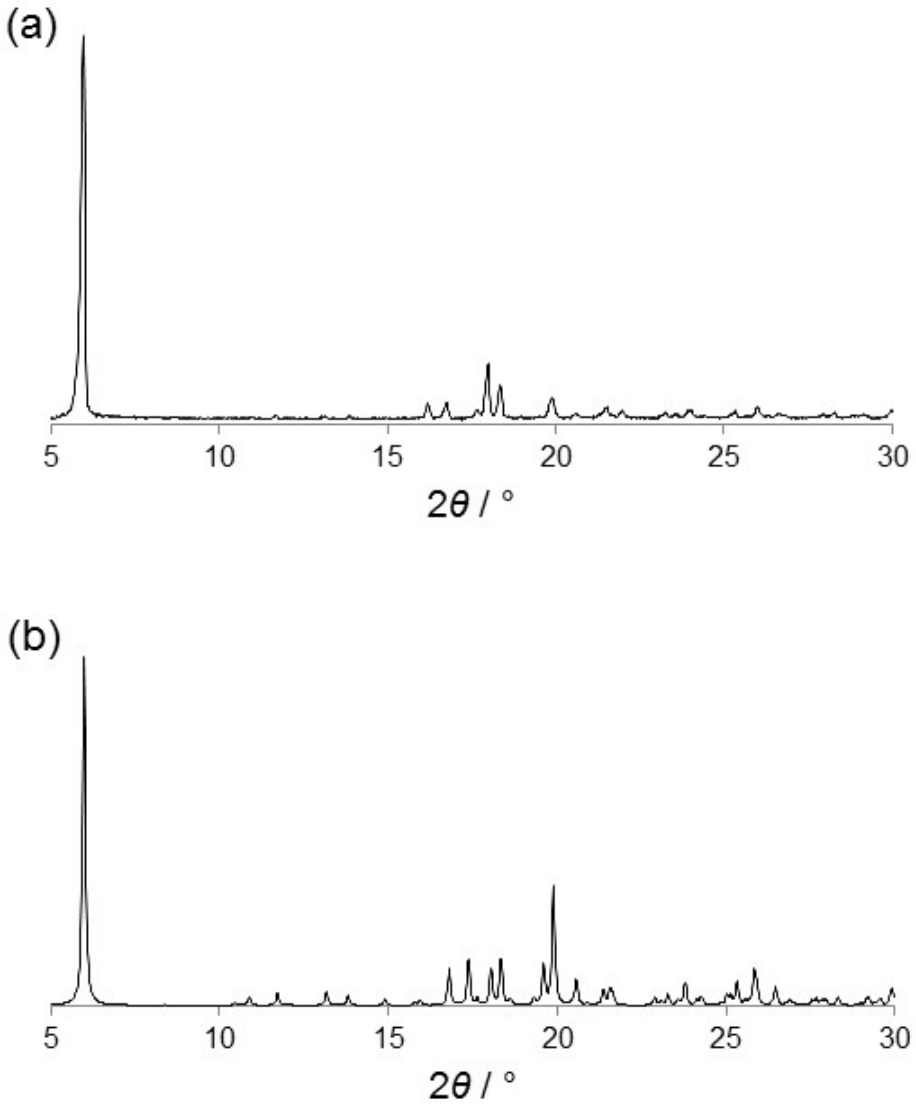

Figure S12. Experimental XRPD of second sphere adduct **1** obtained upon grinding (a) and simulated from its single crystal X-ray structure determination (b).

Synthesis of second sphere adducts 3-5.

Solution method: 0.0346 g (0.5 mmol) **L2** was dissolved into 3 ml dichloromethane in a 50 ml Erlenmeyer flask, then 5 ml methanol, 0.5 mmol MCl_2 (where M is Zn = 0.007 g (**3**); Co = 0.0120 g (**4**); Cd = 0.011 g (**5**)), and one drop of concentrated hydrochloric acid were added, successively. The flask was shaken until the contents dissolved completely and then allowed to stand for about 7 days at room temperature, yielding blue and needle crystal **3** (m. p. 209-212

°C), colorless and needle crystal **4** (m. p. 203-206 °C) and colorless and needle crystal **5** (m. p. 211-217°C).

Grinding method: Two drops of concentrated hydrochloric acid (0.1 mL) was added into ligand **L1** (0.048 g, 0.1 mmol). Then 0.017 g (0.1 mmol) $CuCl_2 \cdot 2H_2O$ was added into the above white powder with the addition of one drop of cyclopentanol. The mixture was ground for about 20 mins until the product became completely dry. During the grinding the color is changed from white to yellow.

Single crystal X- structures of second sphere adducts 3-5.

Crystal structure of second sphere adduct 3. The second coordination sphere adduct **3** crystallizes in the monoclinic $P2_1/c$ space group. In the asymmetric unit, there is one molecule of double protonated **L2** and one $[ZnCl_4]^{2-}$ anion. The double protonated ligand **L2** is interacting via N−H···Cl interactions with one $[ZnCl_4]^{2-}$ anion giving rise to the *quasi*-chelating motif. The geometry of this interactions are *i* and *ii* as follows: *i*) N1-H1···Cl2 with distance $d_{N1\cdots Cl2}$ = 3.116 Å and angle N1-H1···Cl2 = 155°; *ii*) N2-H2···Cl3 with distance dN2···Cl3 = 3.142Å and angle N2-H2···Cl3 = 177°].

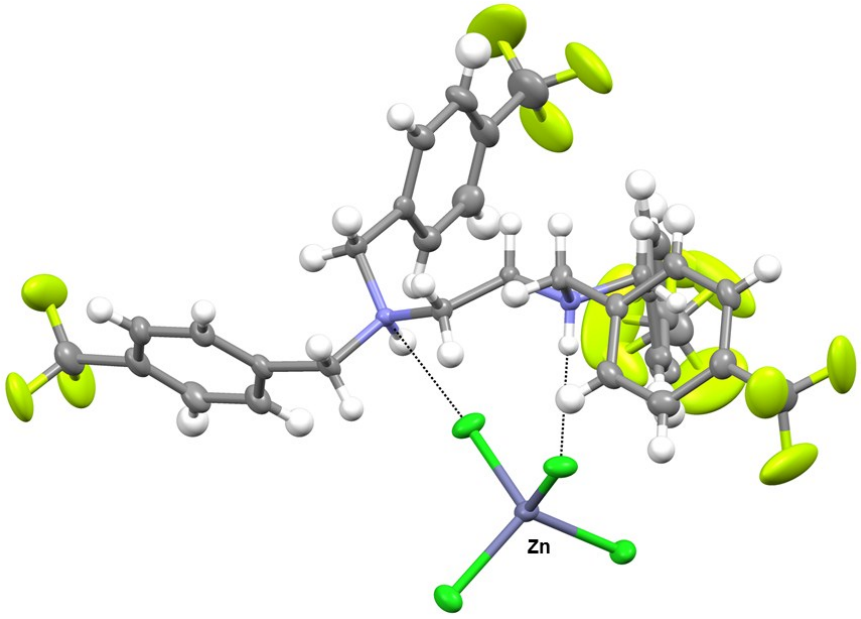

Figure S13. Crystal structure of **3** showing the *quasi*-chelating interaction between the cation and anion. Hydrogen bonding interactions are shown in black dashed lines.

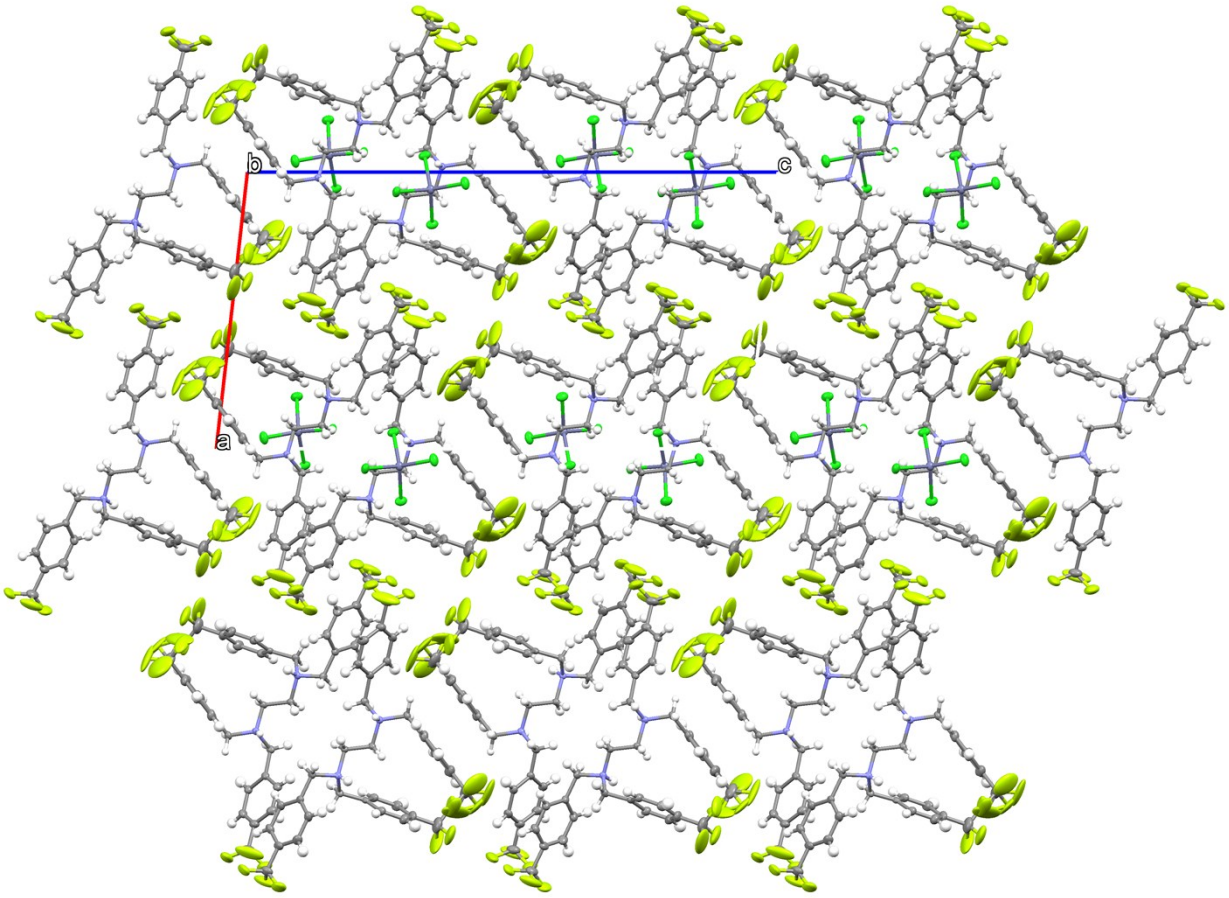

Figure S14. Crystal structure of **3** viewed along the *b*-crystallographic axis.

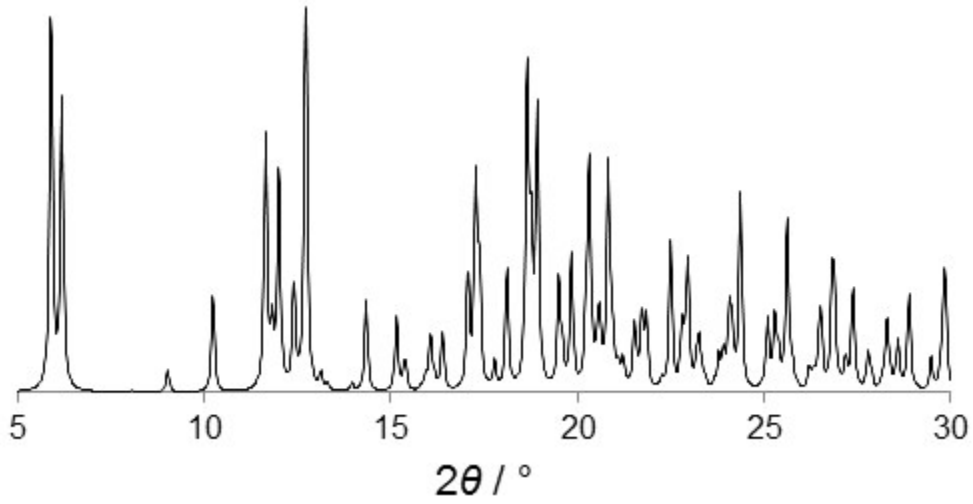

Figure S15. Simulated XRPD pattern of **3** obtained from its single crystal X-ray structure.

Crystal structure of second sphere adduct 4. The second coordination sphere adduct **4** crystallizes in the monoclinic $P2_1/c$ space group. In the asymmetric unit, there is one molecule of double protonated **L2** and one $[CoCl_4]^{2-}$ anion. As observed in second sphere adducts **2** and **3**, in **4** the double protonated ligand **L2** is interacting via N−H···Cl interactions with one $[CoCl_4]^{2-}$ anion giving rise to the *quasi*-chelating motif. The geometry of these interactions *i* and *ii* are as follows: *i*) N1−H1···Cl1 with distance $d_{N1\cdots Cl2}$ = 3.132 Å and angle N1−H1···Cl1 = 161°; *ii*) N2−H2···Cl3 with distance dN2···Cl3 = 3.152Å and angle N2−H2···Cl3 = 168°].

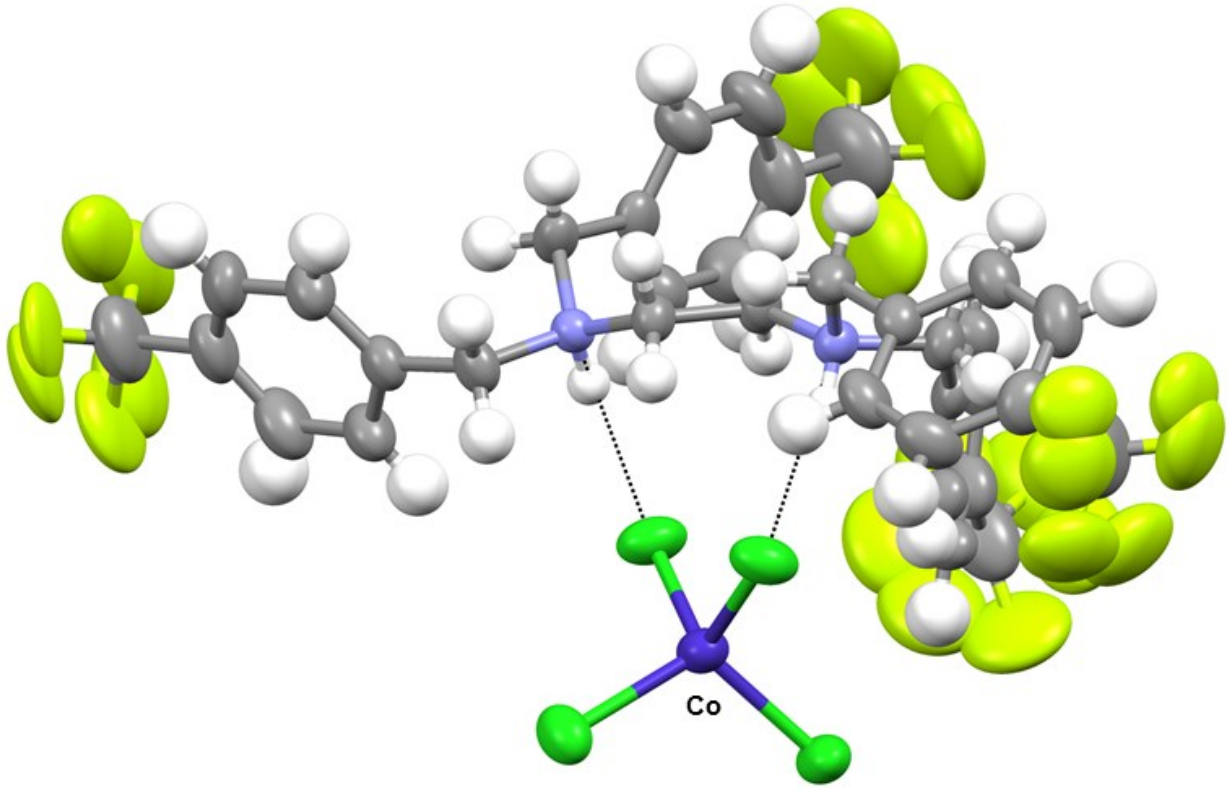

Figure S16. Crystal structure of **4** showing the *quasi*-chelating interaction between the cation and anion. Hydrogen bonding interactions are shown in black dashed lines.

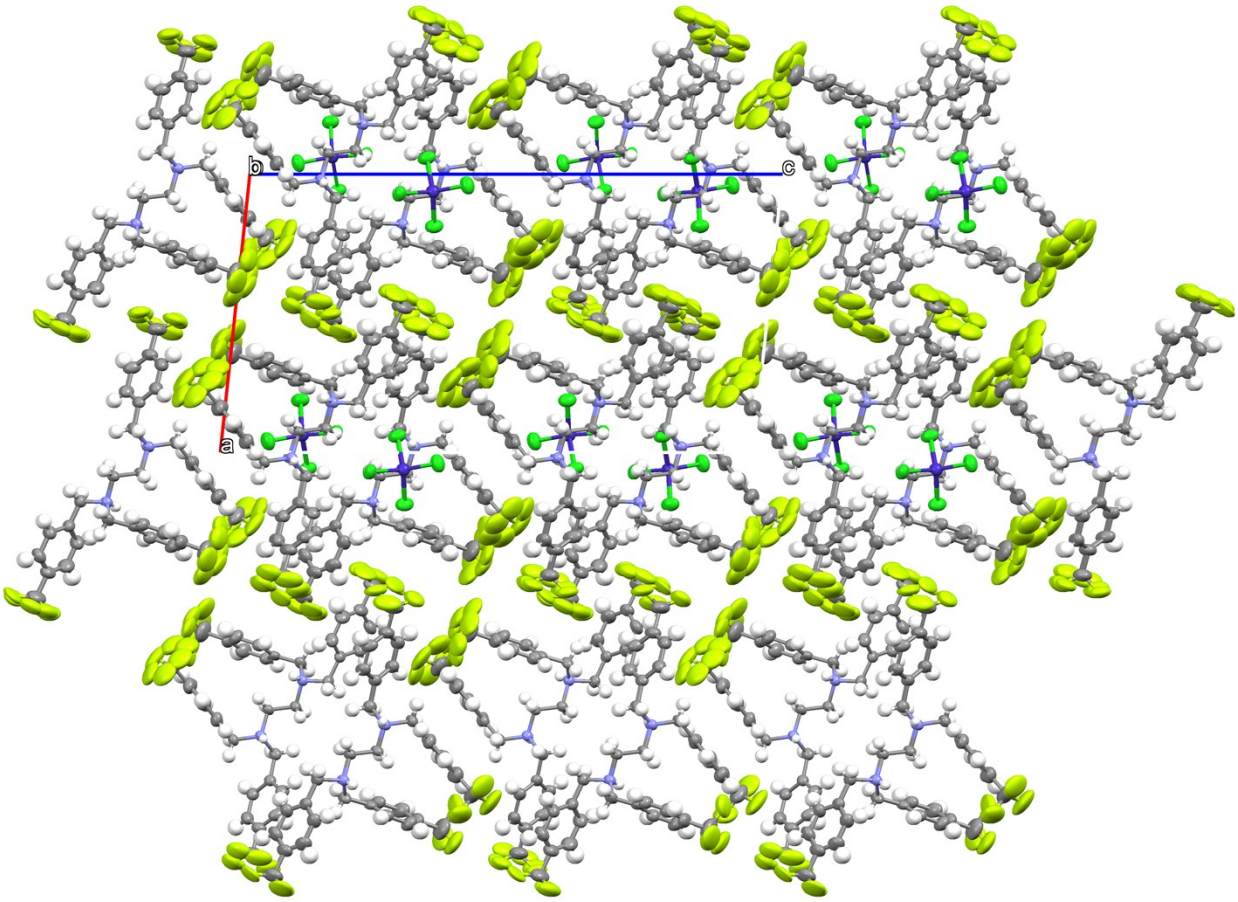

Figure S17. Crystal structure of **4** viewed along the *b*-crystallographic axis.

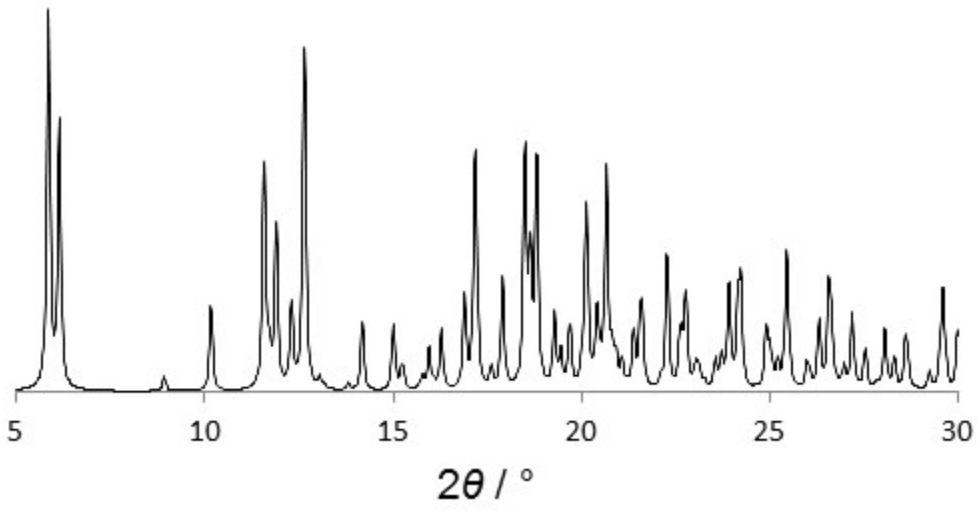

Figure S18. Simulated XRPD pattern of **4** obtained from its single crystal X-ray structure.

Crystal structure of second sphere adduct 5. The second coordination sphere adduct **5** crystallizes in the monoclinic $P2_1/c$ space group. In the asymmetric unit, there is one molecule of double protonated **L2** and one $[CdCl_4]^{2-}$ anion. The *quasi*-chelating interaction between the ion and the cation is also seen in the second sphere adduct **5**. In this case the geometry is also similar to the previously reported by means of two hydrogen bonds via N−H···Cl interactions with one $[CdCl_4]^{2-}$. The geometry of the hydrogen bonds is *i*) N1−H1···Cl2 with distance $d_{N1\cdots Cl2}$ = 3.120 Å and angle N1−H1···Cl2 = 156°; *ii*) N2−H2···Cl4 with distance dN2···Cl4 = 3.134Å and angle N2−H2···Cl4 = 178°].

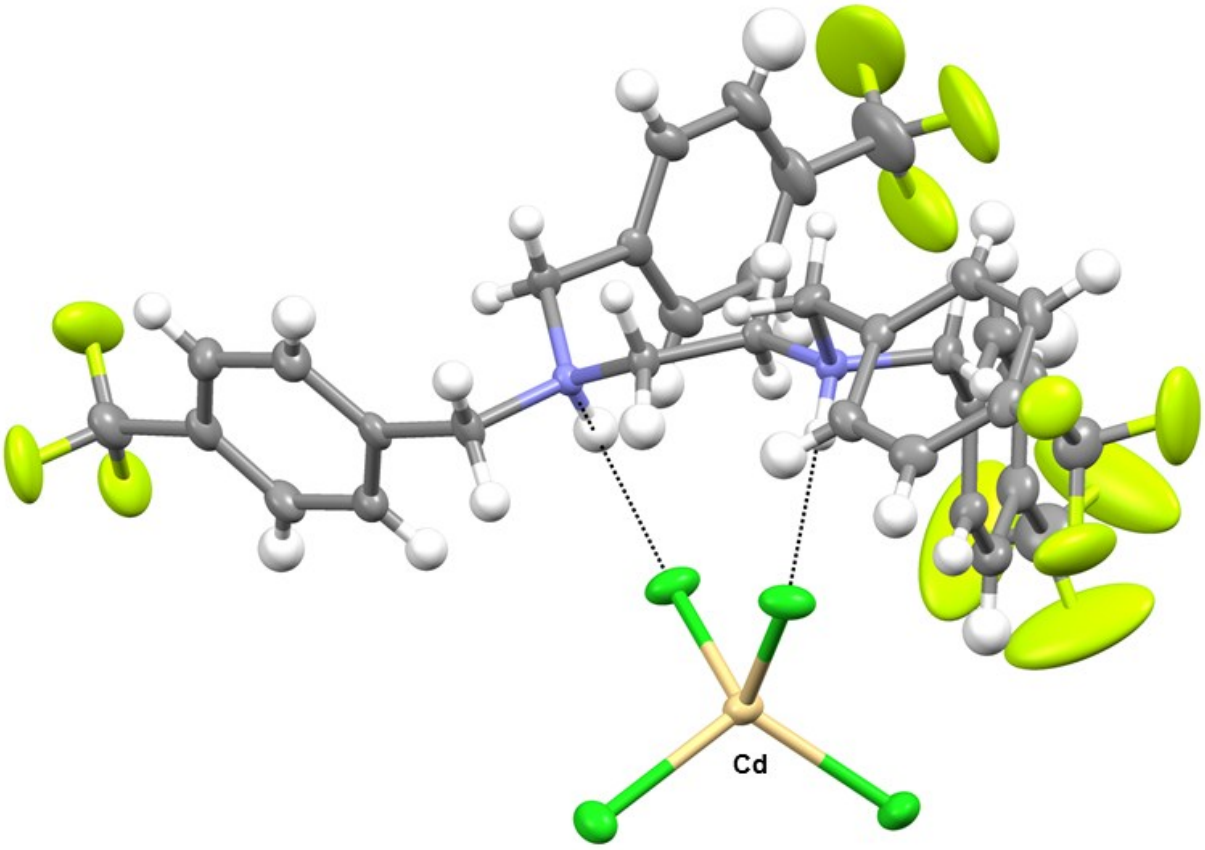

Figure S19. Crystal structure of **5** showing the *quasi*-chelating interaction between the cation and anion. Hydrogen bonding interactions are shown in black dashed lines.

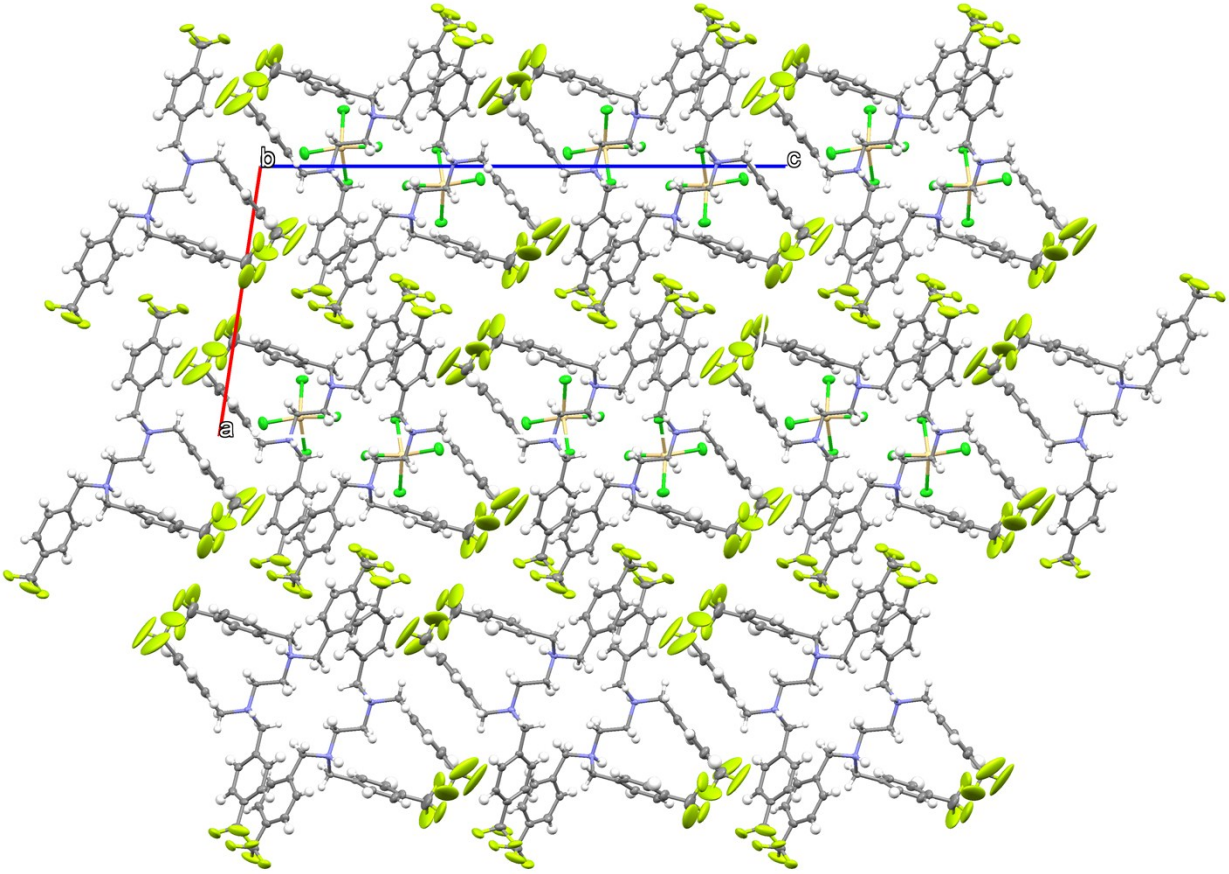

Figure S20. Crystal structure of **5** viewed along the *b*-crystallographic axis.

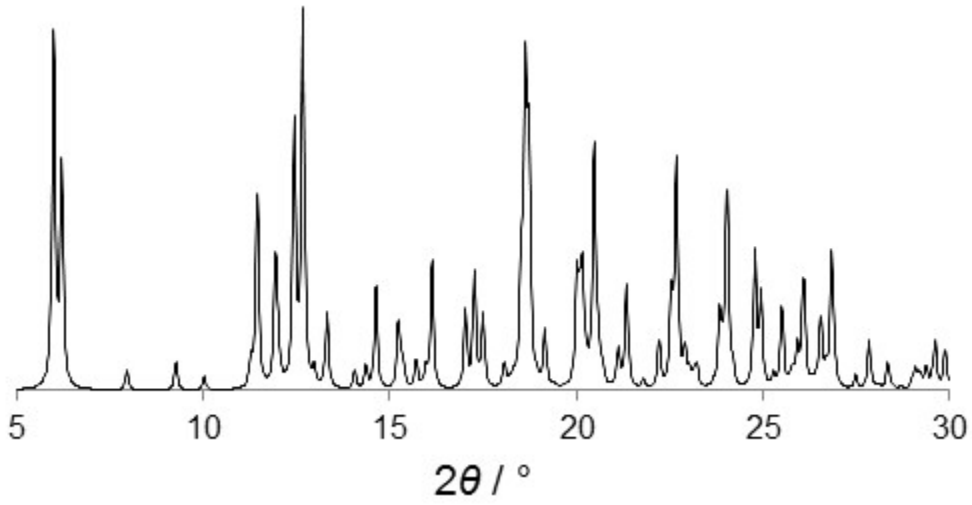

Figure S21. Simulated XRPD pattern of **5** obtained from its single crystal X-ray structure.

LAG using 2 in presence of KOH/K_2CO_3.

Microcrystalline **2** 0.0297g (0.033 mmol), KOH 0.0037g (0.066 mmol) were placed into planetary ball mill, then one drop of EtOH was added. The number of balls in the ball mill were: ϕ 10 mm: 3, ϕ 6 mm: 4; the speed was 120 rpm, frequency is 10Hz, voltage is 56V. The LAG experiments were carried out for periods of ball milling covering 5, 10, 15 and 20 seconds.

From the experimental results an amorphous material is the resulting phase as shown in Figure S22.

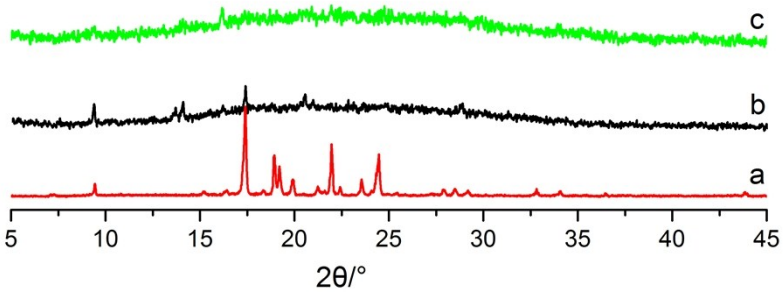

Figure S22. (a) Experimental XRPD pattern of **L2**. (b). LAG of **2** with KOH for 5s. (c). LAG of **2** with KOH for 10s. The product is amorphous.

However, instead changing KOH for K_2CO_3 resulted in a crystalline product.

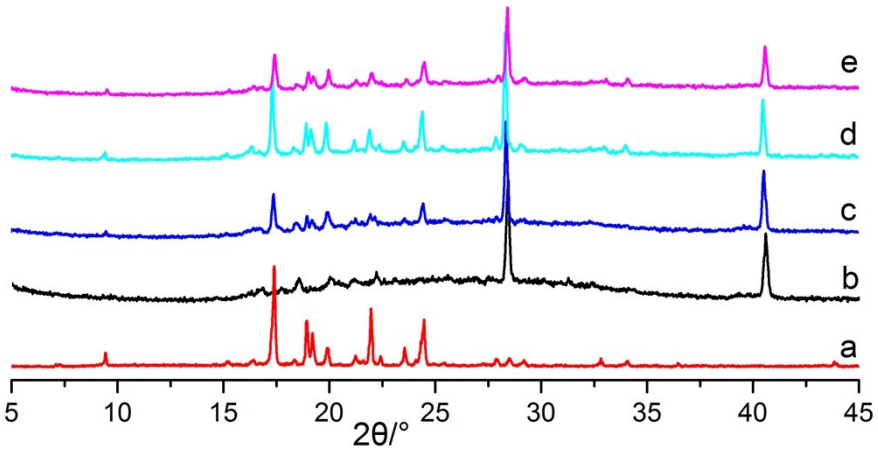

Figure S23. Experimental XRPD pattern of **L2**. (b) LAG of **2** with K_2CO_3 for 5s. (c) LAG of **2** with K_2CO_3 for 10s. (d) LAG of **2** with K_2CO_3 for 15s. (e) LAG of **2** with K_2CO_3 for 20s.

LAG using 3 in presence of KOH/K_2CO_3.

Microcrystalline powders of **3** (0.030 mmol), KOH (0.060 mmol) were placed into planetary ball mill, then one drop of EtOH was added. The number of balls in the ball mill were: ϕ 10 mm: 3, ϕ 6 mm: 4; the speed was 120 rpm, frequency is 10Hz, voltage is 56V. The LAG experiments were carried out for periods of ball milling covering 5, 10, 15 and 20 seconds.

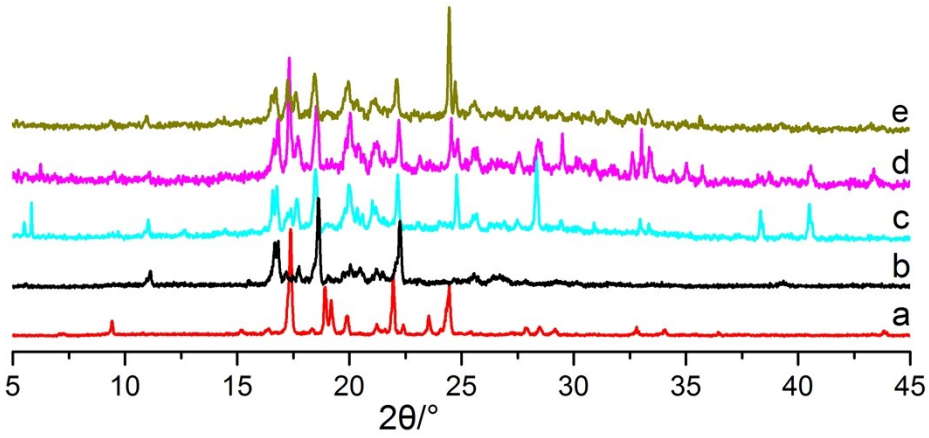

Figure S24. (a) Experimental XRPD pattern of **L2**. (b) Experimental pattern of block new polymorph of ligand **L2** (beta phase). (c) LAG of **3** with KOH for 5s. (d) LAG of **3** with KOH for 10s. (e) LAG of **3** using KOH for 15s.

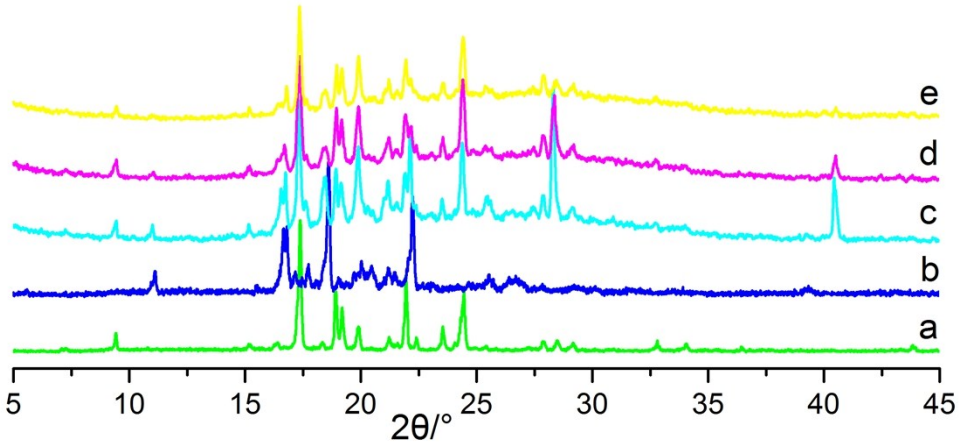

Figure S25. (a) Experimental pattern of **L2**. (b) Experimental pattern of new polymorph. (c) LAG of **3** with K_2CO_3 for 5s. (d) LAG of **3** grind with K_2CO_3 for 10s. (e) LAG of **3** grind with K_2CO_3 for 15s.

LAG using 4 in presence of KOH/K_2CO_3.

Powders of **4** (0.030 mmol), KOH (0.060 mmol) were placed into planetary ball mill, then one drop of EtOH was added. The number of balls in the ball mill were: 3, ϕ 6 mm: 4; the speed was 120 rpm, frequency is 10Hz, voltage is 56V. The LAG experiments were carried out for periods of ball milling covering 5, 10, 15 and 20 seconds.

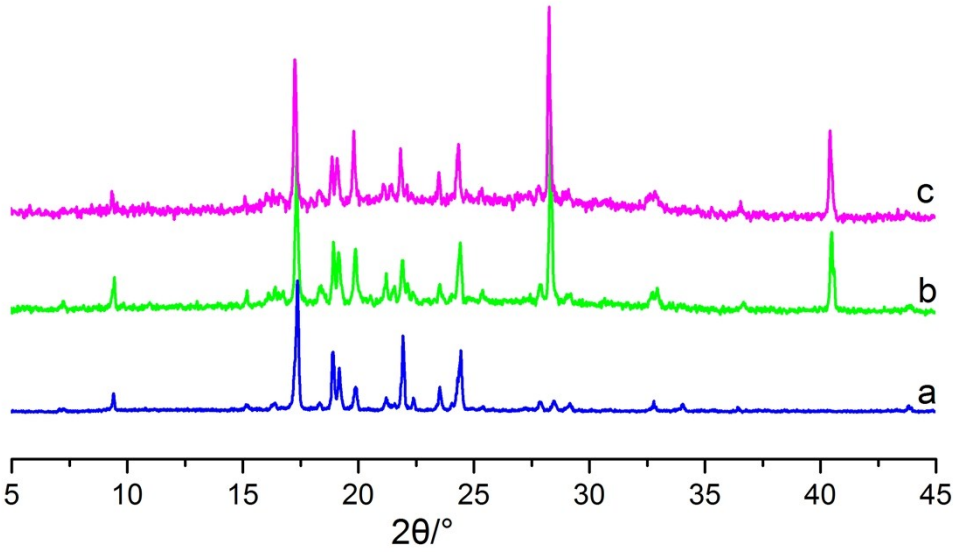

Figure S26. (a) Experimental XRPD pattern of ligand **L2**. (b) LAG of **4** with KOH for 5s. (c) LAG of **4** with KOH for 10s.

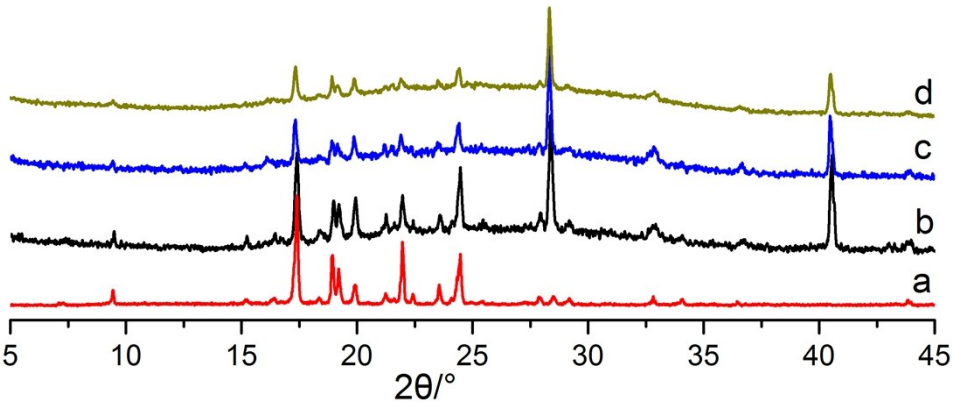

Figure S27. (a) Experimental XRPD pattern of ligand **L2**. (b) LAG of **4** with K_2CO_3 for 5s. (c) LAG of **4** with K_2CO_3 for 10s. (d) LAG of **4** with K_2CO_3 for 15s.

LAG using 5 in presence of KOH/K_2CO_3.

Microcrystalline **5** (0.030 mmol), KOH (0.060 mmol) were placed into planetary ball mill, then one drop of EtOH was added. The number of balls in the ball mill were: 3, Φ 6 mm: 4; the speed was 120 rpm, frequency is 10Hz, voltage is 56V. The LAG experiments were carried out for periods of ball milling covering 5, 10, 15 and 20 seconds.

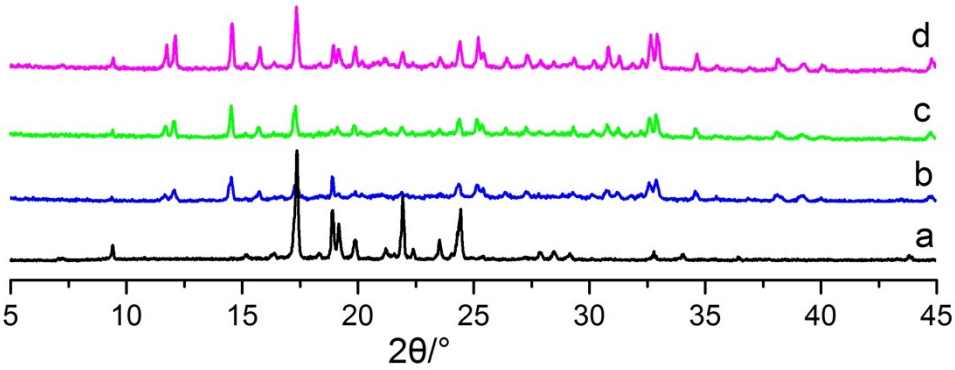

Figure S28. (a) Experimental XRPD pattern of ligand **L2**. (b) LAG of **5** with KOH for 5s. (c). LAG of **5** with KOH for 10s. (d) LAG of **5** using KOH for 15s.

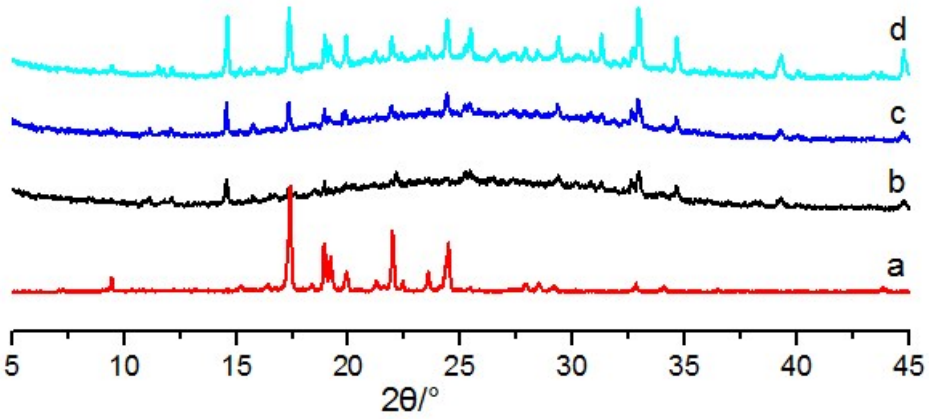

Figure S29. (a) Experimental XRPD pattern of ligand **L2**. (b) LAG of **5** with K_2CO_3 for 5s. (c) LAG of **5**using K_2CO_3 for 10s. (d) LAG of **5** with K_2CO_3 for 15s.

1 a) Sheldrick, G. M. SHELXTL Reference Manual, Siemens Analytical X-ray Systems, Inc.,

Madison, Wisconsin, USA 1996; b) Sheldrick, G. M. *Acta Cryst*. **2008**, A64, 112.
2 Sheldrick, G. M. SHELXTL Version 2014/7. http://shelx.uni-ac.gwdg.de/SHELX/index.php.